Chapter 4

Heterogeneous base catalyst derived from waste sugarcane bagasse for production of biodiesel

4.1 Introduction

"Sugarcane (*Saccharum officinarum*) belonging to the Poaceae family is a strong growing tall perennial grass, which is extensively cultivated across the world as an important commercial crop, particularly in tropical and subtropical regions. It has been reported that sugarcane was planted for the first time in India, and the prime countries that cultivate sugarcane are Brazil, India, and Cuba (Nandhini and Padmavathy, 2017), and after Brazil, India is the second-largest country in planting sugarcane and producing sugar (Pandey et al., 2000; Antunes et al., 2019). Globally, the annual production of sugarcane is estimated to be 1.6 billion tons approximately which are mainly used for the production of sugar and ethanol (by fermentation), and Brazil, the largest producer of sugarcane in the world, produced approximately 635.51 million tons of sugarcane in the year 2018–2019 (Schmitt et al., 2020). However, the sugarcane produced in India was approximately 376.9 million tons in the year 2017–2018 (Niju et al., 2019). It has been reported that the raw sugarcane is mainly composed of 10–16 % fiber (cellulose, pentose and lignin) and 84–90 % broth of which 75–82 % is water and 10–25 % is soluble solids (Canilha et al., 2012). The soluble solids contain 15.5–24 % of sugar such as sucrose (14.5–24 %), glucose (0.2–1 %) and fructose (0–0.5 %), and also contain non-sugar part (1–2.5 %) which are organic compounds (0.8–1.8 %) such as wax, amino acids, starch, phenolic compounds, organic acids, etc. and inorganic components (0.8–1.8 %) such as K_2O, Fe_2O_3, P_2O_5, SiO_2, etc. (Canilha et al., 2012). Sugarcane is also well-known for juice consumption obtained from its stalk. The fibrous residue of sugarcane known as sugarcane bagasse has wide applications (Canilha et al., 2012; Sahiron et al., 2017; Loh et al., 2013). Sugarcane bagasse has a strong potential for biogas production as well (Eshore et al., 2017). Chen et al. (2017) transesterified the sugarcane bagasse to transform it into sustainable bioplastics. Mokhena et al. (2017) also studied sugarcane bagasse fiber for the production of polymeric materials. Sugarcane bagasse has also been reported for the generation of electricity and production of value-added products like paper, pulp, etc. (Pandey et al., 2000; Sangnark and Noomhorm, 2004). Sugarcane bagasse ash was reported for ammoniacal nitrogen removal

from the landfill leachate (Mor et al., 2019), application in ceramic floor tile (Schettino and Holanda, 2015) and for making cementitious or brick materials (Rajput and Gupta, 2016; Xu et al., 2019; Shafiq et al., 2016). Chin et al. (2012) reported the preparation of a solid acid catalyst from sugarcane bagasse by carbonization and sulfonation. The catalyst was tested for its activity in the esterification of palm fatty acid distillate and a maximum of 80 % methyl esters was reported using 11.5 wt. % of catalyst loading and 20 wt. % of methanol ratios at 170 ^{o}C in 30 min. Flores et al. (2019) prepared an acid catalyst through carbonization-sulfonation from sugarcane bagasse and utilized it for oleic acid esterification with methanol. Niju et al. (2019) synthesized biochar from sugarcane bagasse through activation-carbonization and it was reported as a catalyst for transesterification of waste cooking oil with 98.94 % biodiesel conversion using the catalyst amount of 10 wt. % and 2:1 MTOMR at 65 °C in 2 h. Augustia et al. (2018) prepared biochar and utilized it as a catalyst for the esterification reaction of free fatty acids. Ezebor et al. (2014) and Lou et al. (2012) also reported the utilization of heterogeneous acid catalyst which was derived through sulfonation of carbonized sugarcane bagasse for the preparation of biodiesel via an esterification reaction. However, as per the literature survey is concerned, so far, no report has been found about the preparation of heterogeneous base (alkaline) catalyst from the sugarcane bagasse and its catalytic activity for the synthesis of methyl esters (biodiesel). Sugarcane bagasse has strong potentials to be utilized as raw materials for catalyst production over the other types of biomasses as the global sugarcane production is very high and abundant quantities of sugarcane bagasse are generated as waste. In this study, sugarcane bagasse calcined ash material is utilized as a heterogeneous catalyst and its catalytic efficiency for biodiesel synthesis from *Jatropha curcas* oil has been reported for the first time (Basumatary et al., 2021b).

4.2 Experimental

4.2.1 Materials

Waste sugarcane bagasse was collected in May 2019 from the local sugarcane juice vendors of Kokrajhar town, India for the preparation of the catalyst. To examine the catalytic efficiency of the catalyst, *J. curcas* oil, a product of LIFERR^{TM} Naturally Elite, was purchased online from Amazon. The acid value of *J. curcas* oil is determined as 1.307 mg KOH/g. The solvents and chemicals used throughout the investigation were similar as utilized in Chapter **2 (Section 2.2.1, Page no. 34**).

4.2.2 Preparation of sugarcane bagasse calcined catalyst (SBCC)

The collected waste sugarcane bagasse was allowed to dry completely under the sun for 15 days during May 2019. After that the catalyst was prepared by similar procedures as mentioned in Chapter **2 (Section 2.2.2.1, Page no. 34**).

4.2.3 Characterization of SBCC

The characterization of the SBCC catalyst were investigated by using powder XRD, BET, FT-IR, FESEM, EDX, XPS, HRTEM and SAED analytical instruments having the same model number and protocol described in Chapter **2 (Section 2.2.2.2, Page no. 35-36**). The pH value and basicity of SBCC was also measured by following similar procedure as mentioned in Chapter **2 (Section 2.2.2.2, Page no. 36**).

4.2.4 Reaction procedures of transesterification and product characterization

Synthesis of biodiesel from *J. curcas* oil (2 g) was investigated with methanol using SBCC (5, 10, 15 and 20 wt. %). The temperatures at which the catalytic activity was tested were 45, 55, 65 and 75 ^{o}C, and the different methanol to oil molar ratios (MTOMR) employed were 6:1, 9:1, 12:1, and 15:1. The further steps involved in carrying the transesterification reaction are follow as same protocol described in Chapter **2 (Section 2.2.2.3, Page no. 36-37**). The similar equation in Chapter 2 (**Page no. 37**). was also applied to calculate the yield of biodiesel.

J. curcas oil and biodiesel were characterized by the spectra of ^{1}H NMR (400 MHz, $CDCl_3$) recorded on the FT-NMR spectrometer (Bruker Avance II). The chemical composition of biodiesel was determined from GC-MS spectra recorded in the same GC-MS instrument and followed similar procedure as described in Chapter **2** (**Section 2.2.2.3, Page no. 37**). The density (at 29 ^{o}C) of produced biodiesel was measured using the method reported by Basumatary et al. (2014). The specific gravity of biodiesel was determined following ASTM (American Society of Testing and Material) D 1298 and EN (European Standard) ISO 3675 test method (Rupasianghe and Gunathilaka, 2018). The viscosity (at room temperature, 29 ^{o}C) was measured using Ostwald's viscometer following the test method of ASTM standard D445 mentioned by Alptekin et al. (2008). Iodine value (IV) and saponification number (SN) were determined by applying the reported standard equations (Basumatary et al., 2014; Krisnangkura et al., 1991). ASTM D2015 approved standard equations (Adepoju et al., 2018) were employed for the determination of other properties like cetane index, higher heating value (HHV), American petroleum index (API), diesel index, and aniline point.

4.3 Results and Discussion

4.3.1 Characterization of the calcined catalyst

4.3.1.1 Powder XRD analysis

The catalyst (SBCC) was characterized by the powder XRD pattern to find out the qualitative presence of inorganic components. The analysis of the 2θ values of the XRD pattern of the SBCC based on JCPDS data (ICDD 2003) revealed the presence of chloride (KCl), carbonates and oxides. Carbonates are found to be present as K_2CO_3, Na_2CO_3, $MgCO_3$ and $CaMg(CO_3)_2$, and the various oxides present are K_2O, SiO_2, CaO, MgO, ZnO, P_2O_5, SrO and Fe_2O_3 (**Fig. 4.1**). The peaks at 2θ values of 28.39, 40.53, 50.15, 58.65 and 73.71 revealed the presence of KCl, and similar 2θ values for KCl were also reported by Fan et al. (2019) for ash catalyst obtained from waste banana peel. The presence of K_2CO_3 in SBCC can be interpreted from the 2θ values at 29.56, 30.89, 34.02, 40.98 and 42.63. K_2O can be indicated from the 2θ values of 27.97, 39.89 and 56.38. The 2θ values at 20.89, 21.36, 26.64, 36.56, 39.49 and 59.96 are indicating the existence of SiO_2 (quartz). The occurrence of CaO was shown by the peaks at 2θ of 32.37, 37.17, 43.08, 66.43 and 67.77. Accordingly, the presence of Na_2CO_3 can be indicated by the 2θ value of 37.83, and $MgCO_3$ by the 2θ values of 42.45 and 68.37. SrO showed peaks at 2θ values of 28.58 and 30.29, and ZnO showed a peak at 2θ value of 35.91. Similarly, P_2O_5 and Fe_2O_3 can be identified from the 2θ value at 61.04 and 24.37, respectively, and dolomite, $CaMg(CO_3)_2$, showed a peak at 2θ value of 45.0.

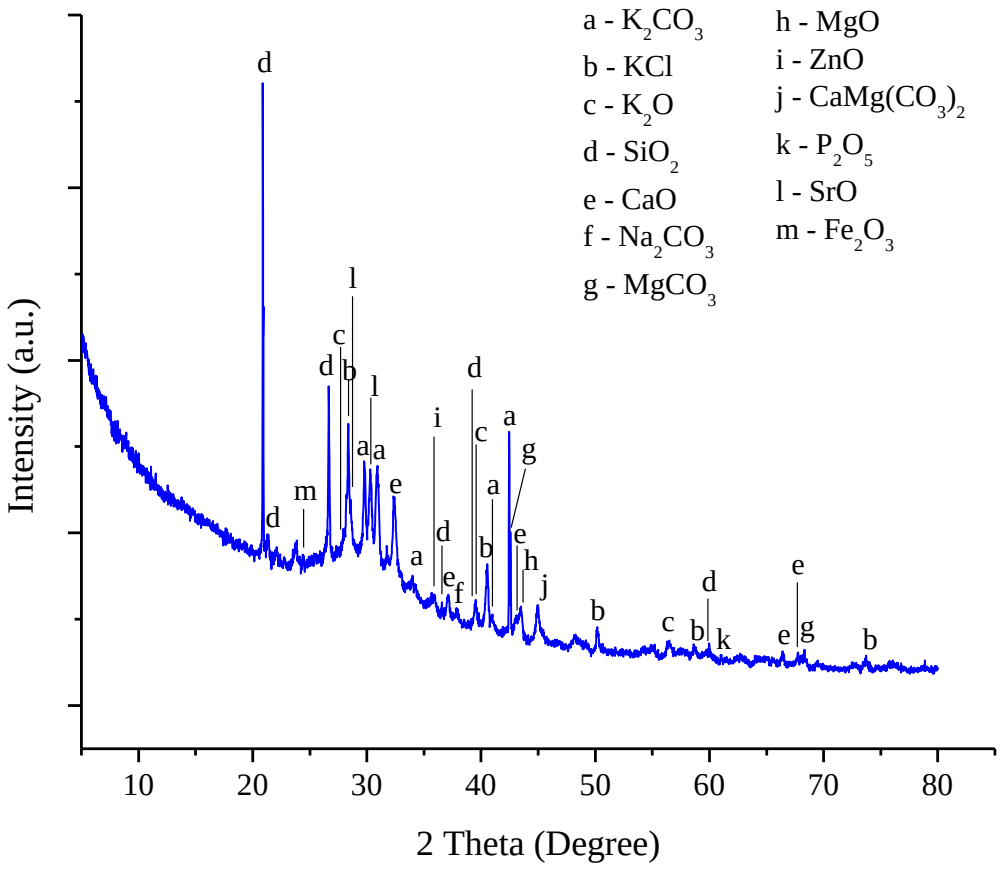

Fig. 4.1. XRD pattern of sugarcane bagasse calcined catalyst (SBCC).

4.3.1.2 FT-IR analysis

The FT-IR spectrum of SBCC is depicted in **Fig. 4.2**. The band at 3450 cm^{-1} ascribes the vibration of O–H bond due to the adsorption of H_2O molecule on the catalyst. The FT-IR peaks at 1640, 1462, 1422 and 1385 cm^{-1} are denoting the stretching frequencies of C–O bond due to the presence of carbonates, which are attributing the existence of metal carbonates in the catalyst. The appearance of a sharp peak at 1043 cm^{-1} is representing Si–O–Si bond vibration, and showing the presence of SiO_2 (Nath et al., 2019). The peak at 783 cm^{-1} appeared may be due to K–O stretching frequency, whereas the peaks at 620 and 565 cm^{-1} may represent Ca–O bond vibration. The FT-IR study supports the presence of SiO_2, K_2O, CaO and K_2CO_3 in the SBCC catalyst as predicted from the XRD pattern. Comparable results of the presence of SiO_2, K_2O, CaO and K_2CO_3 with analogous absorption bands were also reported by Nath et al. (2019), Pathak et al. (2018) and Changmai et al. (2020a).

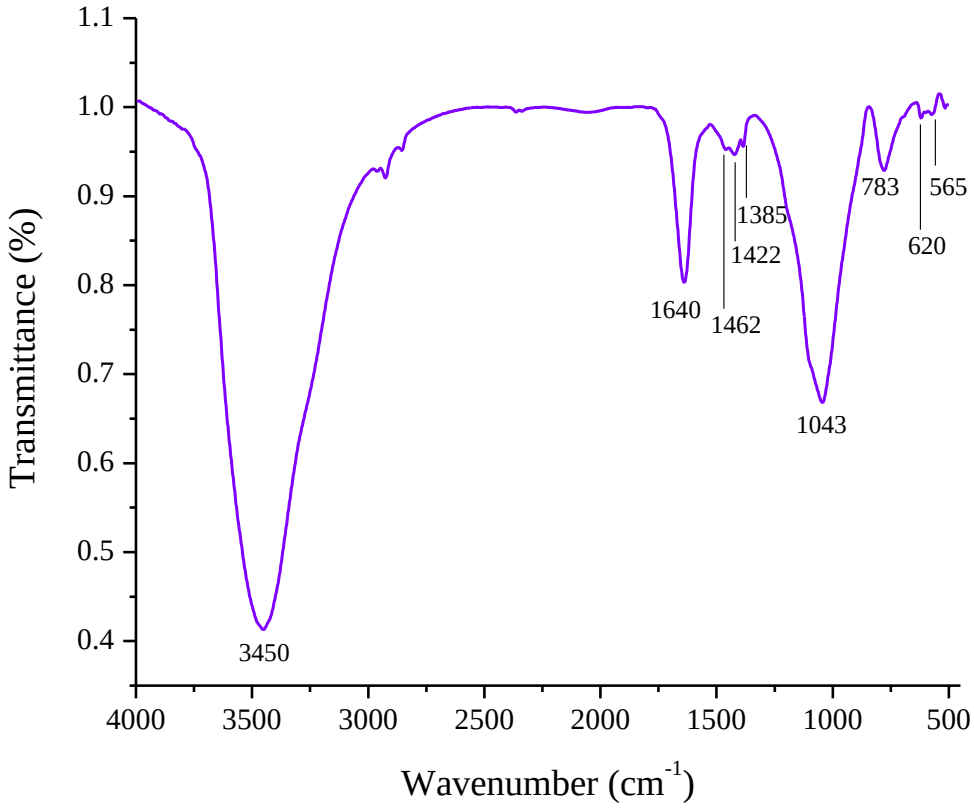

Fig. 4.2. FT-IR spectrum of SBCC.

4.3.1.3 BET analysis

The N_2 adsorption-desorption isotherm and pore size distribution of the catalyst are depicted in **Fig. 4.3** and **Fig. 4.4**, respectively. The isotherm (**Fig. 4.3**) slightly matches with the typical type IV isotherm with characteristics H3 hysteresis loop, representing the mesoporous materials of the catalyst (Pathak et al., 2018; Betiku et al., 2019; Nath et al., 2020). The pore volume of the catalyst is found to be 0.014 $cm^3\ g^{-1}$. The average pore diameter is found to be 2.479 nm, and the pore diameter is ranging from 1.160 nm to 11.101 nm, indicating the borderline micro-mesoporous structure of the catalyst. Nath et al. (2019) reported a catalyst of microporous material derived waste *Brassica nigra* with type I isotherm and a pore diameter of 1.67 nm. Thommes (2010) reported the micro-mesoporous nature of zeolite with similar N_2 adsorption-desorption isotherm. SBCC was measured with a low surface area of 7.66 $m^2\ g^{-1}$ which might be due to the low amount of unburnt carbon-particles present in the catalyst. Mendonça et al. (2019b) reported a low surface area of 1.0 $m^2\ g^{-1}$ for waste tucumã peel catalyst calcined at 800 ^oC. Similarly, Dai et al. (2014) reported low a surface area (1.21 $m^2\ g^{-1}$) for peanut husk catalyst calcined at 900 ^oC. A smaller surface area of 1.454 $m^2\ g^{-1}$ has also been

reported by Pathak et al. (2018) for *Musa acuminate* peel catalyst and it was stated that the catalyst with low unburnt-carbon particle possesses a low surface area.

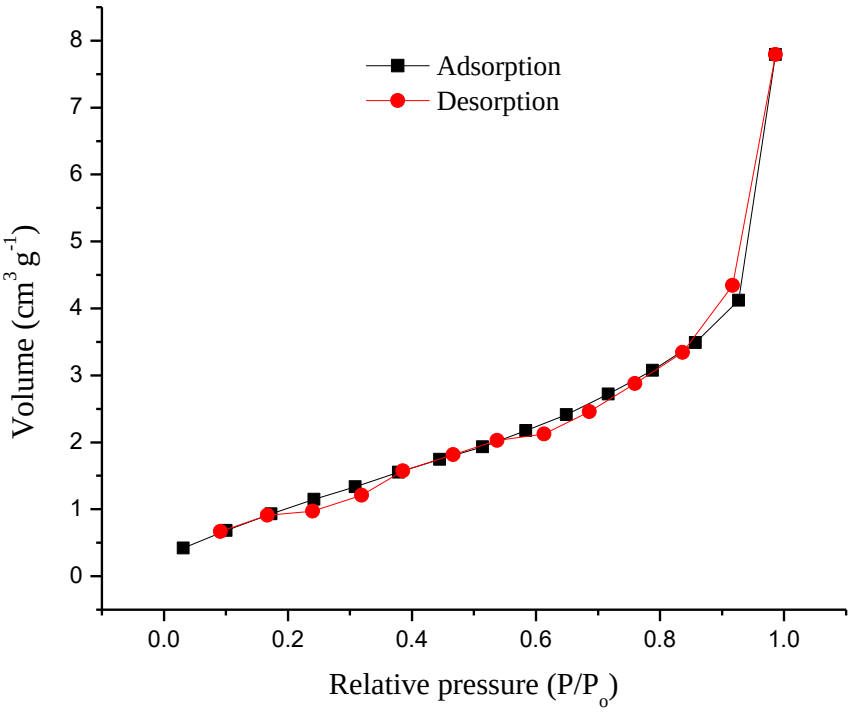

Fig. 4.3. Adsorption-desorption (N_2) isotherm of SBCC.

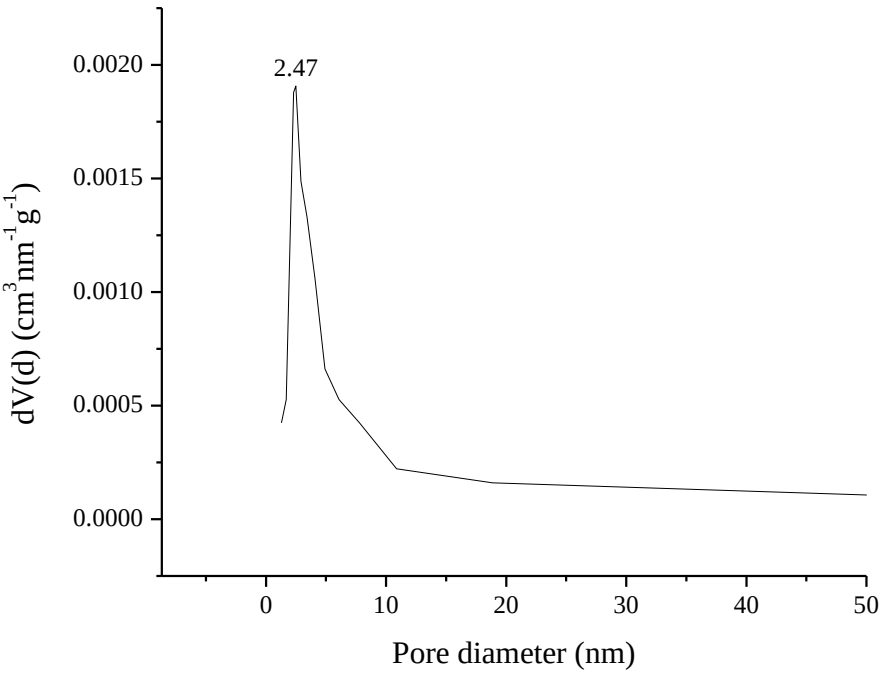

Fig. 4.4. Pore size distribution of SBCC.

4.3.1.4 FESEM and HRTEM analyses

The catalyst was visualized by FESEM and HRTEM micrographs and depicted in **Fig. 4.5** (A–C) and **Fig. 4.6** (A–E), respectively. From FESEM images, the cracked and agglomerated particles of the catalyst were seen with irregular and sheet-like pellets (**Fig.** 4.5 B). In line with FESEM, the HRTEM images also showed the non-uniform (**Fig.** 4.6 A–C) and porous-like structure (**Fig.** 4.6 D, E) of the catalyst. The SAED pattern shown in **Fig.** 4.6 F is indicating the polycrystalline nature of the catalyst. Similarly, Nath et al. (2019) and Talukdar and Deka (2016) reported the polycrystalline nature of the heterogeneous catalysts from waste plants.

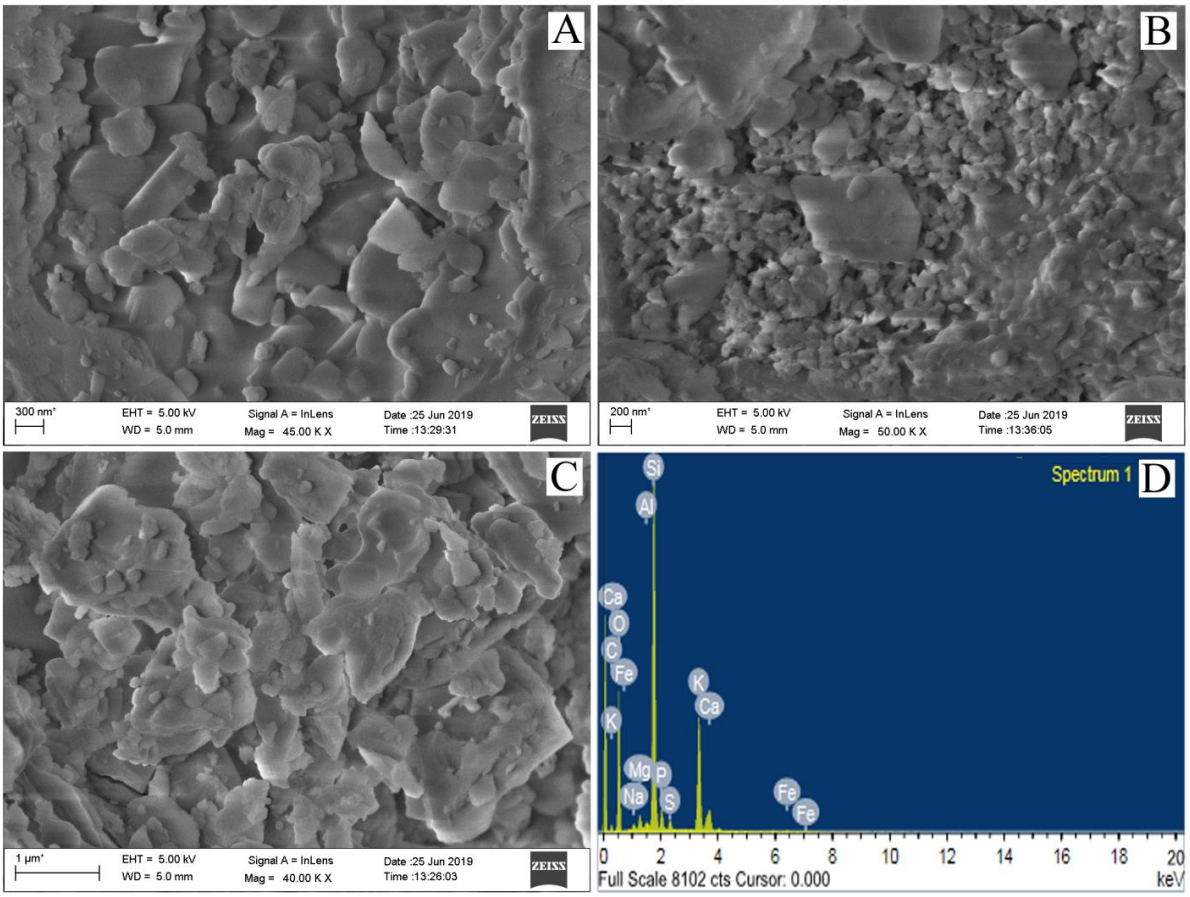

Fig. 4.5. FESEM (A–C) and EDX (D) images of SBCC.

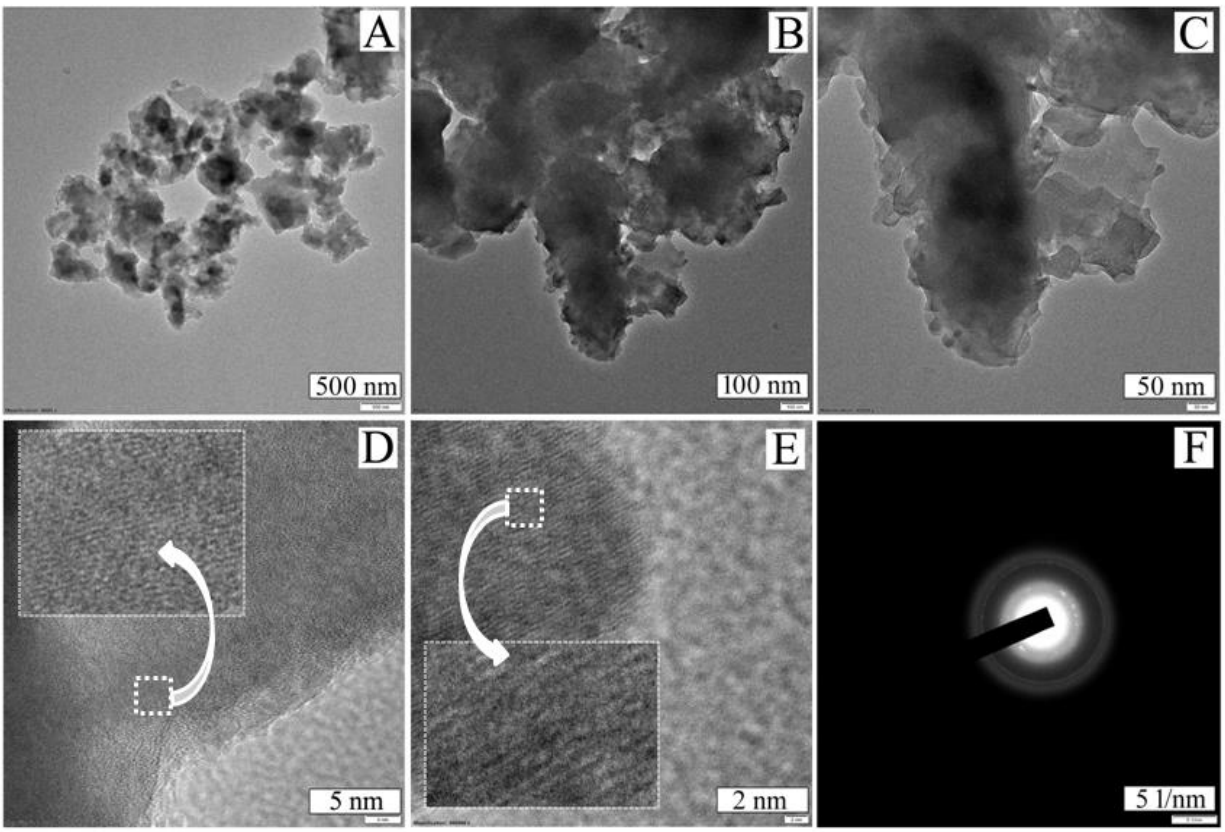

Fig. 4.6. HRTEM images (A–E) and SAED pattern (F) of SBCC.

4.3.1.5 EDX analysis

The FESEM-EDX analysis of the catalyst is shown in **Fig. 4.5** D, and the composition of the elements present are presented in **Table 4.1**. The major elements present are O (50.22 wt. %) > Si (24.11 wt. %) > K (12.07 wt. %) > C (5.89 wt. %). The high amount of O, Si, K and C indicated in EDX analysis confirmed the presence of SiO_2, K_2CO_3 and K_2O, which were predicted during XRD analysis (**Fig. 4.1**). Betiku et al. (2017) and Basumatary et al. (2018) stated that plant wastes-derived catalysts containing high K content possess good catalytic activity, and K in the form of carbonate and oxide along with other active components can effectively catalyze the transesterification of oil to biodiesel.

Table 4.1: FESEM-EDX analysis of sugarcane bagasse calcined catalyst (SBCC).

Elements	Composition of catalyst	
	Weight %	**Atomic %**
C	5.89	9.73
O	50.22	62.27
Si	24.11	17.03
K	12.07	6.12
Ca	2.43	1.20
Mg	1.12	0.91
Na	0.60	0.52
Al	0.24	0.18
P	2.14	1.37
S	0.94	0.58
Fe	0.25	0.09

4.3.1.6 XPS analysis

XPS analysis (**Fig. 4.7**, **Table 4.2**) of the catalyst confirms the presence of the elements in the order of Si > O > C > K > Ca > Sr > Mg > Na > Zn > Mn > Cl > Fe. The higher concentration of Si (38.19 %), O (25.12 %), C (19.78 %) and K (9.49 %) confirmed the existence of XRD predicted components such as SiO_2, K_2CO_3 and K_2O, and were also supported by FT-IR analysis (**Fig. 4.2**). The deconvoluted spectrum of O 1s (**Fig. 4.7** B) with binding energy 531.93 eV is indicating the presence of oxides of metals in the catalyst (Yadav et al., 2017). The analysis is showing binding energy of 284.89 eV in the deconvoluted C 1s spectrum (**Fig. 4.7** C), suggesting the presence sp^2 hybridized carbon of the metal carbonates in the catalyst (Wang et al., 2017). The two peaks in the spectrum of K 2p (**Fig. 4.7** D) with binding energies of 293.21 eV and 295.89 eV are representing K $2p_{3/2}$ and K $2p_{1/2}$ designating the +1-oxidation state of K (Roy et al., 2020b). Similarly, the occurrence of calcium is confirmed by the appearance of peaks with binding energies of 345.97 eV and 349.42 eV (Nath et al., 2019). Si in the form of SiO_2 showed a peak at the deconvoluted Si 2p spectrum (**Fig. 4.7** F) with the binding energy of 102.63 eV (Nath et al., 2020).

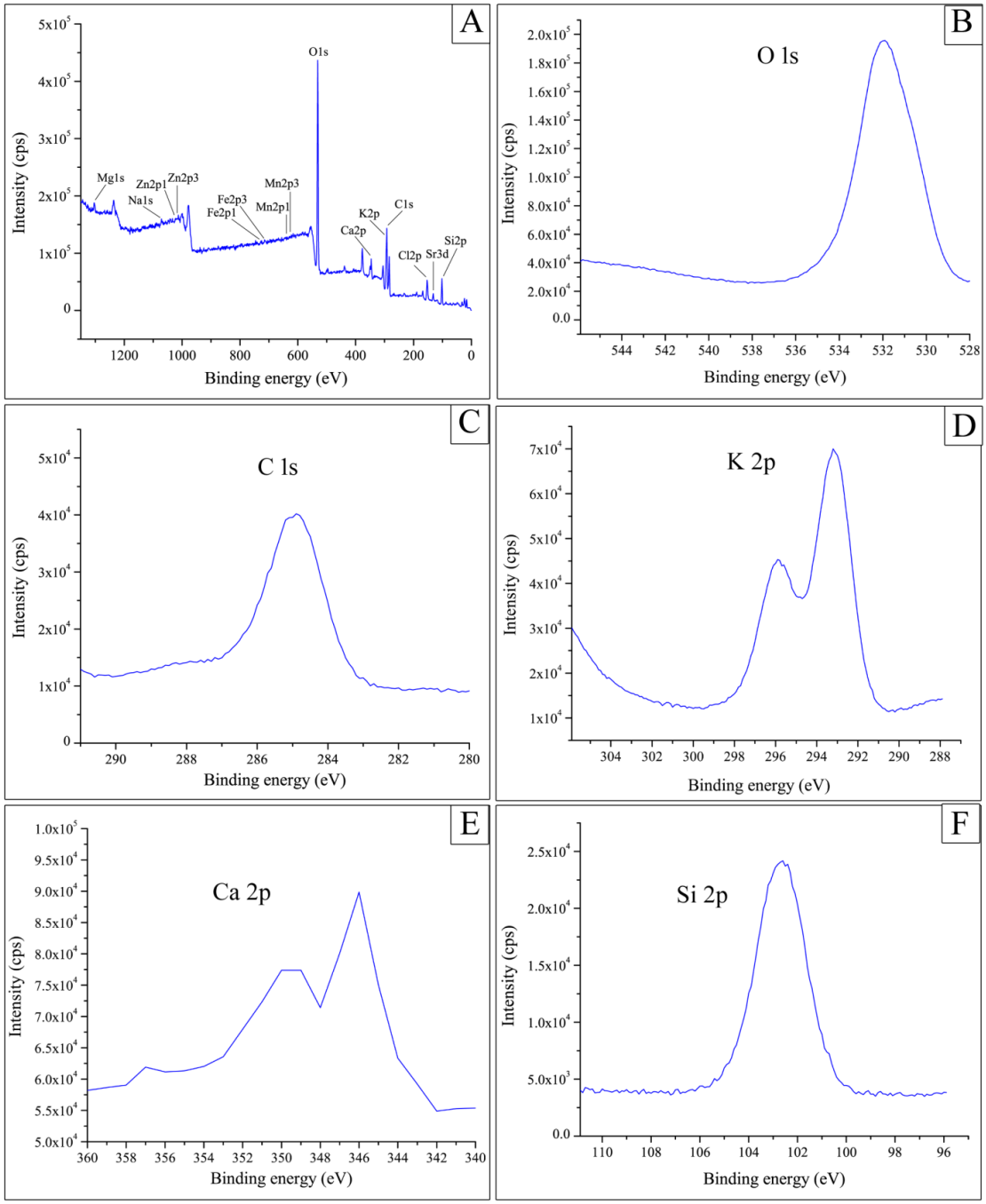

Fig. 4.7. XPS spectra of SBCC (A–Survey plot, B–O 1s, C–C 1s, D–K 2p, E–Ca 2p, and F–Si 2p).

Table 4.2: XPS analysis of SBCC.

Elements	**Composition of catalyst (Atomic %)**
C 1s	19.78
O 1s	25.12
Si 2p	38.19
K 2p	9.49
Ca 2p	4.22
Mg 1s	0.41
Na 1s	0.40
Mn 2p	0.32
Zn 2p	0.36
Fe 2p	0.21
Sr 3d	1.19
Cl 2p	0.31

4.3.1.7 pH value determination

The pH value of the catalyst dissolved in distilled water at different ratios (w/v) was measured and the observed change in pH value with dilution has been shown in **Fig. 4.8**. It is seen that the pH values at 1:5 (w/v) and 1:40 (w/v) are 12.10 and 11.62, respectively indicating a gradual decrease in the basic nature of the catalyst with dilution. From the measured pH values, it can be envisaged that the sugarcane catalyst has remarkable basicity.

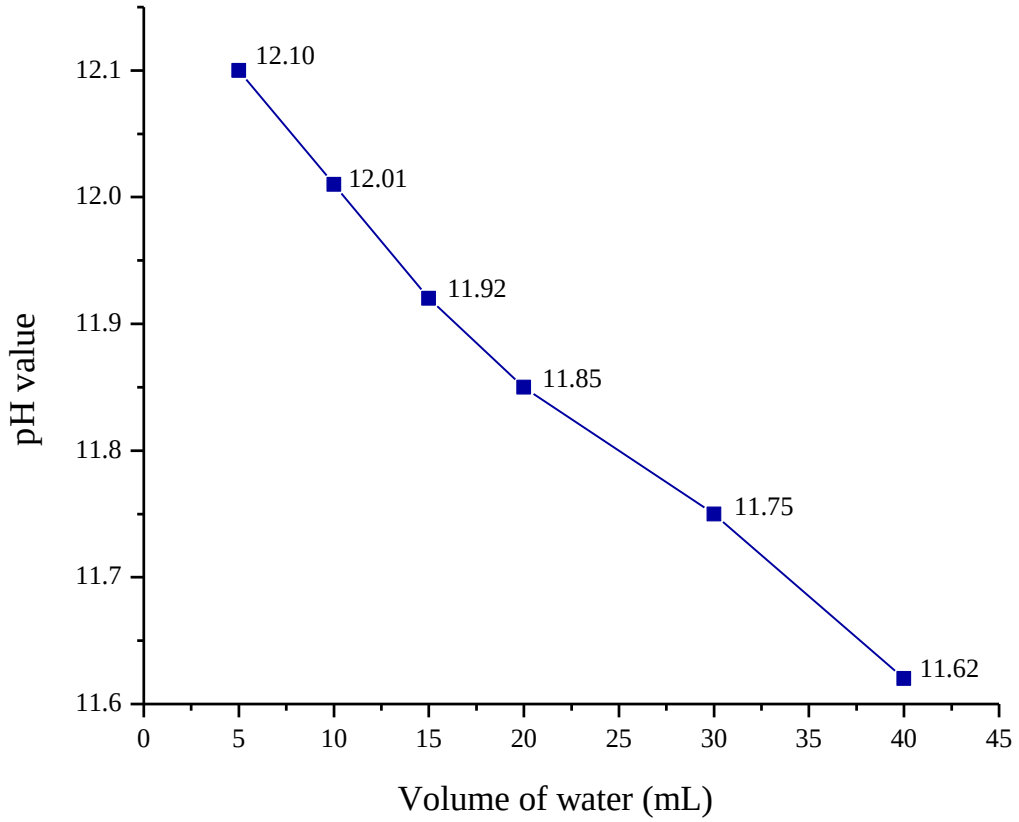

Fig. 4.8. pH value of 1 g SBCC dissolved in different volumes of distilled water (w/v).

4.3.1.8 Determination of basicity of catalyst and turnover frequency

The basicity of the SBCC was studied using the Hammett indicators. During the experiments, a color change from blue to green in the case of bromothymol blue (H_ = 7.2), pink to colorless in case of phenolphthalein (H_ = 9.3) and deep pink to magenta with nile blue solution (H_ = 10.1) was observed. But the catalyst is unable to change the color of the methanolic solution of 4-nitroaniline (H_ = 18.4) and aniline (H_ = 27.0) indicators against the benzoic acid solution (0.01 M). Thus, the basic strength range of SBCC is found within 10.1 < H_ < 18.4, and the basicity of the catalyst was estimated to be 0.0891 mmol g^{-1}. Using the basicity result, the turnover frequency (TOF) of the catalyst was calculated (Roy et al., 2020b) from equation (4.1). The TOF significantly gives information about the efficacy of the catalyst. The calculated TOF value of SBCC is 6.59 h^{-1}. However, a lower TOF of 4.29 h^{-1} was reported by Roy et al. (2020c) in biodiesel synthesis using K promoted La_2O_3 solid catalyst.

$$\text{TOF} = \frac{\text{Moles of produced biodiesel}}{\text{Basicity (mmol)} \times \text{time (sec)}} \qquad (\mathbf{4.1})$$

4.3.2 Study of catalytic activity in the conversion of *J. curcas* oil to biodiesel

4.3.2.1 Effect of catalyst loading

The efficiency of SBCC with respect to the amount of oil was investigated by varying the catalyst concentration keeping the MTOMR (9:1) and temperature (65 ^{o}C) fixed, and experimental results are shown in **Fig. 4.9**. The scrutiny of the catalyst loading reveals that 390 min of reaction time with 5 wt. % catalyst decreases significantly to 285 min with increasing catalyst loading to 10 wt. % along with the significant increase in the product yield from 88.52 to 92.84 wt. %. However, no substantial increase in the yield of biodiesel is noticed beyond 10 wt. % of catalyst loading. The probable reason for this may be because of the excess amount of catalyst that resists the mass transfer in heterogeneous catalysis, adsorbs the reactants and it may increase the viscosity of the reaction system, and as a result, the interaction of the reactant molecules is suppressed leading to the loss of the product (Pathak et al., 2018; Changmai et al., 2020a; Fatimah et al., 2019).

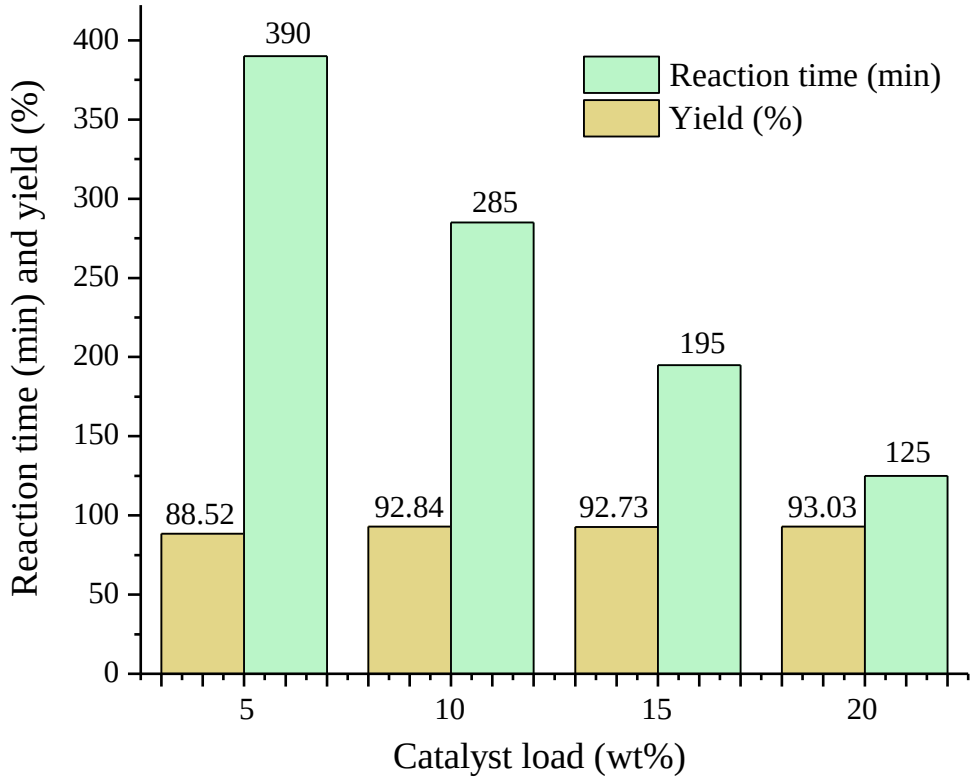

Fig. 4.9. Effect of SBCC loading on production of biodiesel (Temperature = 65 ^{o}C, MTOMR = 9:1).

4.3.2.2 Effect of MTOMR

Optimum MTOMR is an essential factor in the competent synthesis of biodiesel. Though stoichiometrically 3:1 MTOMR is required in the conversion of the feedstock into biodiesel, a higher molar ratio can shift the equilibrium towards the product and is considerably preferred for higher product yield (Laskar et al., 2018). The efficacy of the reaction with MTOMR was investigated at 65 ^{o}C using 10 wt. % of catalyst loading. It can be viewed from the result (**Fig. 4.10**) that the time taken for completion of the reaction is almost comparable with different MTOMR used. However, the yield of biodiesel increases from 89.35 to 92.84 wt. % with increasing MTOMR from 6:1 to 9:1. Beyond 9:1 MTOMR, when the reaction is tested with MTOMR of 12:1 and 15:1, no increase in the yield of product is noticed, instead, a slight decrease of product yield is observed (**Fig. 4.10**). This may be due to dilution of the reaction mixture with increased concentration of methanol leading to less interaction of catalyst with reactant molecules. Thus, MTOMR of 9:1 is considered as the optimum ratio for biodiesel synthesis in the present study.

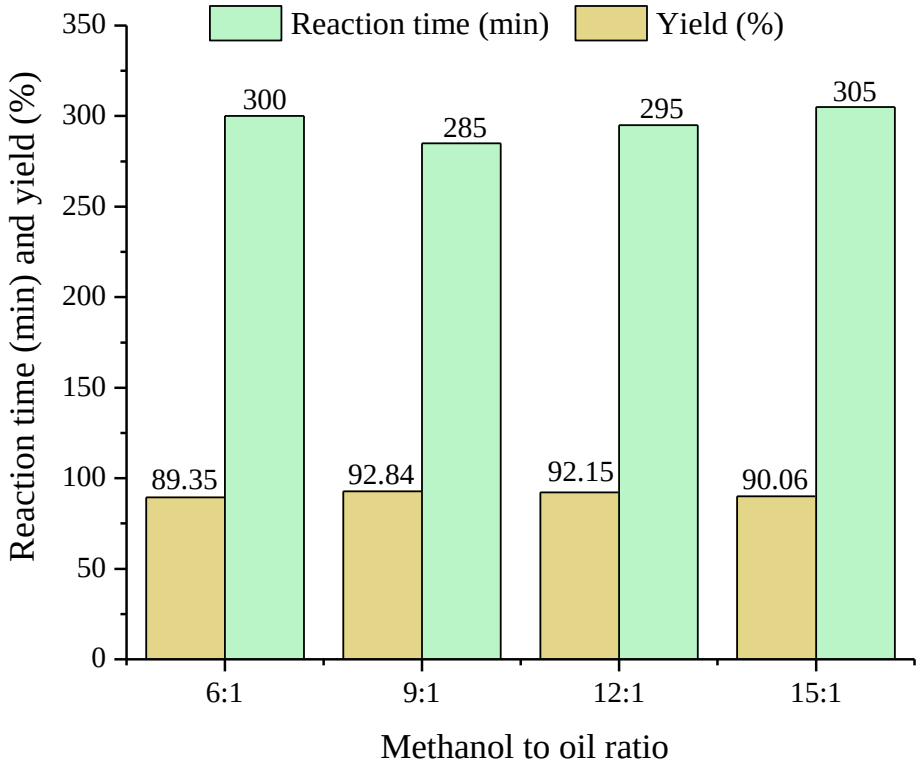

Fig. 4.10. Effect of MTOMR on production of biodiesel (Temperature = 65 ^{o}C, catalyst dose = 10 wt.%).

4.3.2.3 Effect of temperature on synthesis of biodiesel

The influence of temperature on the conversion of *J. curcas* oil to biodiesel was studied using MTOMR of 9:1 and 10 wt. % catalyst amount and the results are depicted in **Fig. 4.11**. It has been observed that increase in reaction temperature from 45 ^{o}C to 55 ^{o}C and then to 65 ^{o}C, the time taken for reaction completion significantly decreases from 480 min (45 ^{o}C) to 285 min (65 ^{o}C). Further increase of temperature to 75 ^{o}C, reaction time does not decrease noticeably (**Fig. 4.11**). The reaction time required for the experiment is high. This may be due to the low potassium (12.07 wt.%) and calcium (2.43 wt.%) contents in the catalyst compared to other biomass-based catalysts such as *Brassica nigra* (Nath et al., 2019), *Sesamum indicum* (Nath et al., 2020), tucumã peels (Mendonça et al., 2019b) and cocoa pod husks (Betiku et al., 2017; Ofori-Boateng and Lee, 2013) which have higher alkali metal contents. On increasing temperature from 45 ^{o}C to 65 ^{o}C, biodiesel yield increases from 89.13 to 92.84 wt. %. However, when the temperature is raised to 75 ^{o}C, no further increase in the yield of the product is noticed. In this study, the best results in terms of reaction time and product yield are obtained at 65 ^{o}C, which may be due to enrichment in adequate kinetic energy to achieve the energy barrier for the conversion of triglycerides to esters (Sahani and Sharma, 2018). Further, the vaporization of methanol initiates beyond 65 °C and methanol escapes from the reaction mixture, and as a result, there will be a lower concentration of methanol causing less interaction with the triglyceride and catalyst (Sahani and Sharma, 2018; Li et al., 2018). Therefore, 65 ^{o}C is chosen as the temperature for transesterification of *J. curcas* oil to biodiesel at 9:1 MTOMR and 10 wt. % of catalyst.

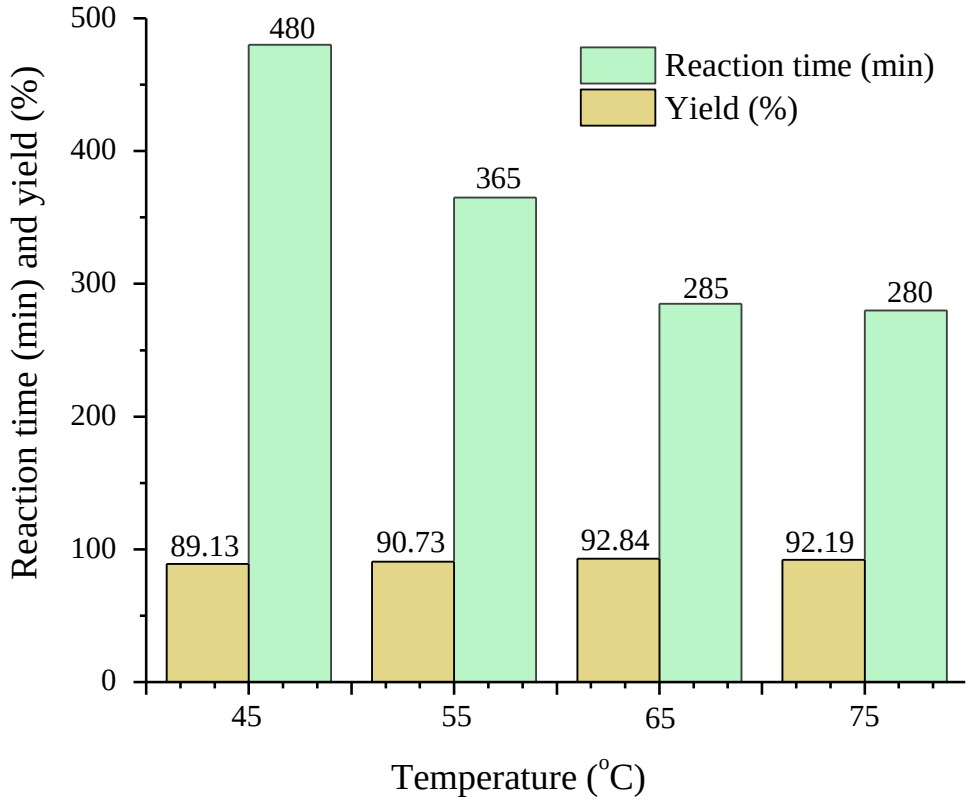

Fig. 4.11. Effect of temperature on production of biodiesel (MTOMR = 9:1, catalyst dose = 10 wt.%).

4.3.2.4 Reusability of catalyst

The reusability test of the catalyst (SBCC) has been executed based on the procedures reported earlier (Nath et al., 2020) under the conditions of 9:1 MTOMR and 10 wt. % of catalyst at 65 ^{o}C. The result is shown in **Fig. 4.12**. In the first reusability test, 89.76 wt. % biodiesel was achieved in 475 min, and in the second cycle of reaction, 83.65 wt. % yield of biodiesel was achieved in 690 min. The result of reusability indicates that the effectiveness of the catalyst is decreased gradually after every reaction cycle. This gradual decrease in catalytic activity may be due to loss of catalyst or leaching of some active components during the catalyst recovery processes (Pathak et al., 2018; Nath et al., 2020).

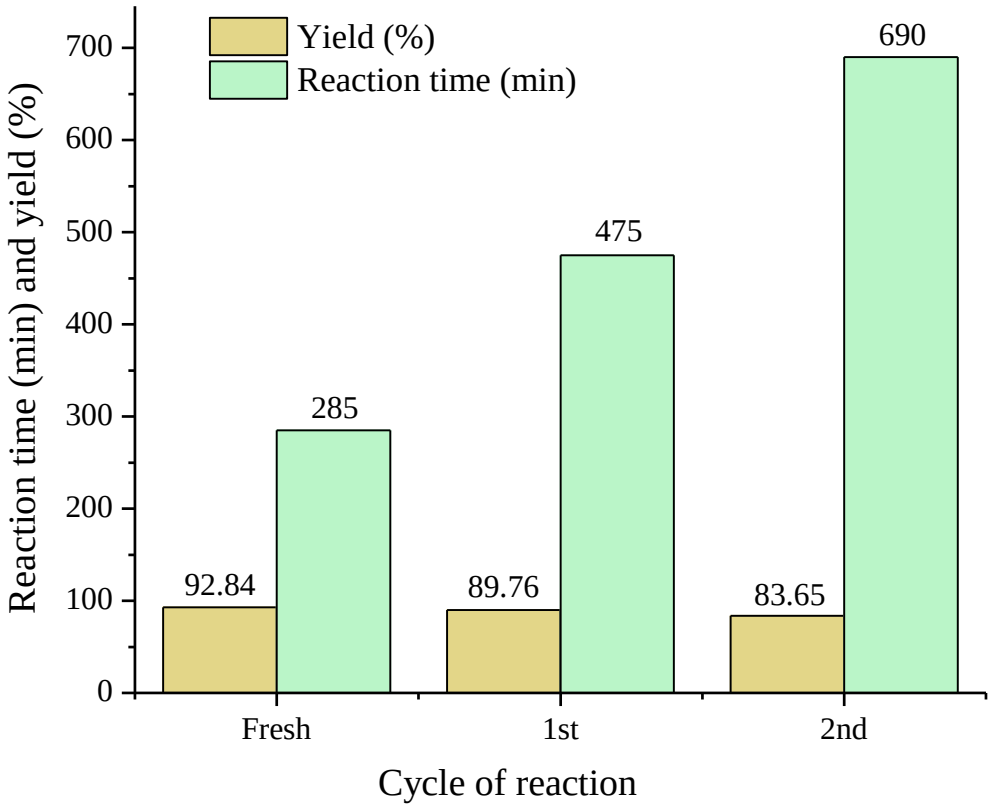

Fig. 4.12. Reusability of SBCC on production of biodiesel (Temperature = 65 ^{o}C, MTOMR = 9:1, catalyst dose = 10 wt.%).

4.3.3 Kinetic study of the reaction

Principally, heterogeneous catalyzed transesterification of triglyceride (oil) with methanol to fatty acid methyl esters (FAME) proceeds through the reversible reaction in three consecutive steps in which one mole of glyceride, stoichiometrically, reacts with the three moles of methanol (Roy et al., 2020b; Roy et al., 2020c; Yahya et al., 2018; Nath et al., 2023) as shown below.

$$\text{Triglyceride} + \text{Methanol} \rightleftharpoons \text{FAME} + \text{Diglyceride} \quad (\mathbf{4.2})$$

$$\text{Diglyceride} + \text{Methanol} \rightleftharpoons \text{FAME} + \text{Monoglyceride} \quad (\mathbf{4.3})$$

$$\text{Monoglyceride} + \text{Methanol} \rightleftharpoons \text{FAME} + \text{Glycerol} \quad (\mathbf{4.4})$$

$$\text{Triglyceride} + 3\,\text{Methanol} \rightleftharpoons 3\,\text{FAME} + \text{Glycerol} \quad (\mathbf{4.5})$$

In this study, the kinetics of transesterification of *J. curcas* oil with methanol using SBCC was studied from the data obtained by carrying the reaction at different temperatures such as 45, 55, 65 and 75 ^{o}C under the optimum reaction conditions of MTOMR and catalyst loading. Firstly, the results obtained from the reaction were fitted in the kinetic equations of the zero

order (**4.6**), first order (**4.7**), pseudo-first order (**4.8**) and second order (**4.9**) reactions and then calculated the rate constants (k).

$$\text{For Zero order reaction, } k = \frac{[TG]_o - [FAME]}{t} \quad (\mathbf{4.5})$$

$$\text{First order reaction, } k = \frac{2.303}{t}\log\frac{[TG]_o}{[FAME]} \quad (\mathbf{4.6})$$

$$\text{Pseudo-first order reaction, } k = -\frac{2.303}{t}\log\{1 - [FAME]\} \quad (\mathbf{4.7})$$

$$\text{Second order reaction, } k = \frac{1}{t} \times \frac{2.303}{([TG]_o - a)}\log\frac{a([TG]_o - x)}{[TG]_o(a - x)} \quad (\mathbf{4.8})$$

where, $[TG]_o$ = initial concentration of triglyceride, [FAME] = concentration of product obtained at time 't', x = $[TG]_o$ – [FAME] at time 't', a = initial concentration of methanol {~9 × $[TG]_o$ based on equation (**4.5**)}.

The rate constants calculated for various kinetics models at different temperatures are presented in **Table 4.3**. Using these data, Arrhenius plots are drawn by plotting the value of ln k against the inverse of absolute temperature (1/T) and are depicted in **Fig. 4.13–4.16**. The linear fitting of the plots gives a straight line with the correlation coefficient (R^2 value) of 0.80061 for zero order, 0.73045 for first order, 0.84095 for pseudo-first order and 0.72146 for second order reaction. The best fitted graph (**Fig. 4.15**) with the highest correlation coefficient (R^2 = 0.84095) directs the prediction of the order of the reaction. Accordingly, the transesterification reaction using sugarcane bagasse calcined catalyst is considered to follow pseudo-first order kinetics. Similarly, Kumar and Ali (2013), Kaur et al. (2018), Yahya et al. (2018) and Farid et al. (2018) stated that the transesterification process for biodiesel synthesis with excess methanol obeys pseudo-first order reaction.

From the Arrhenius plot of the predicted pseudo-first order reaction (**Fig. 4.15**), the value of activation energy (E_a) and pre-exponential factor (A) was calculated from the slope (= E_a/R) and intercept (= ln A) of the straight line, respectively. Here, 'R' is the universal gas constant (8.314 J K^{-1} mol^{-1}) and 'T' is the reaction temperature in kelvin. The value of slope was found to be –2660.5, and therefore, the activation energy was calculated to be 22119.39 J mol^{-1} (22.12 kJ mol^{-1}). Similarly, the value of intercept was –1.0436 and therefore, the pre-exponential factor (A) was found to be 3.52 × 10^{-1} s^{-1}. A higher E_a value of 61.23 kJ mol^{-1} was reported by Mendonça et al. (2019b) for the reaction of the tucumã peel catalyzed transesterification process compared to that of the present study. The E_a value of the present study was found within the E_a value of 21–84 kJ mol^{-1}, reported for the catalyzed transesterification process of biodiesel synthesis (Nath et al., 2019; Kumar and Ali, 2013; Kaur et al., 2018).

Table 4.3: Rate constant (k), correlation coefficient (R^2), activation energy (Ea) and pre-exponential factor (A) of various kinetic models.

Order of reaction	**Rate constant, k (s^{-1}) at various temperature (K)**				**R^2 value**	**Activation energy, E_a (kJ mol^{-1})**	**Pre-exponential factor, A (s^{-1})**
	318	328	338	348			
Zero order	3.77×10^{-6}	4.23×10^{-6}	4.19×10^{-6}	4.65×10^{-6}	0.80061	nd	nd
First order	4.00×10^{-6}	4.44×10^{-6}	4.35×10^{-6}	4.84×10^{-6}	0.73045	nd	nd
Pseudo-first order	7.71×10^{-5}	1.09×10^{-4}	1.54×10^{-4}	1.52×10^{-4}	0.84095	22.12	3.52×10^{-1}
Second order	4.47×10^{-7}	4.96×10^{-7}	4.85×10^{-7}	5.40×10^{-7}	0.72146	nd	nd

nd–not determined.

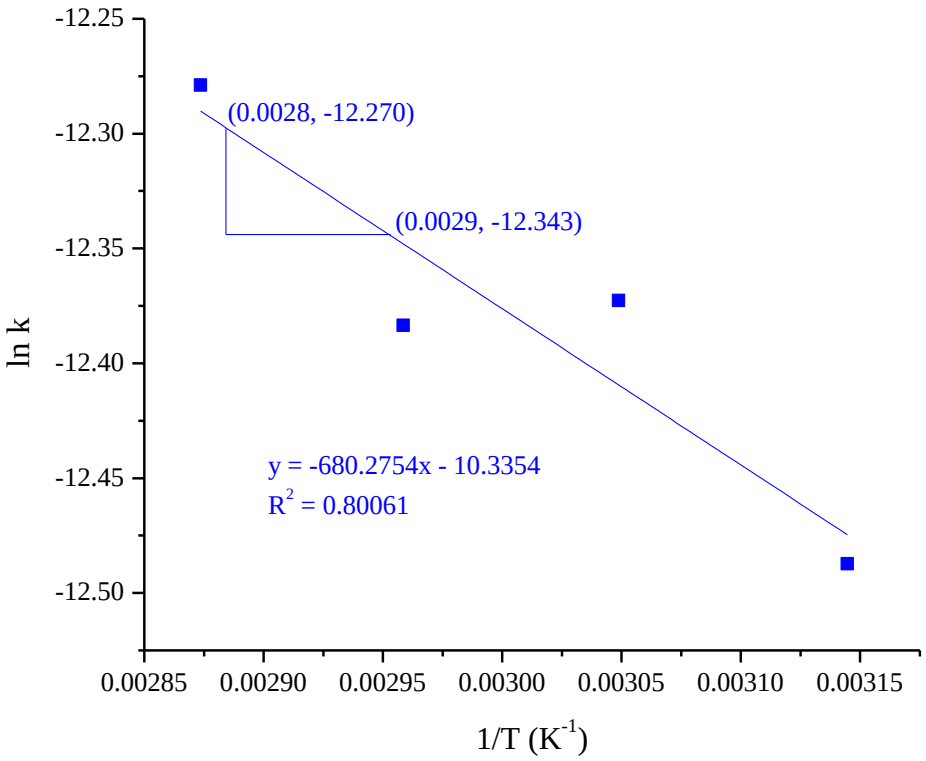

Fig. 4.13. Arrhenius plot (ln k versus 1/T) for zero order reaction.

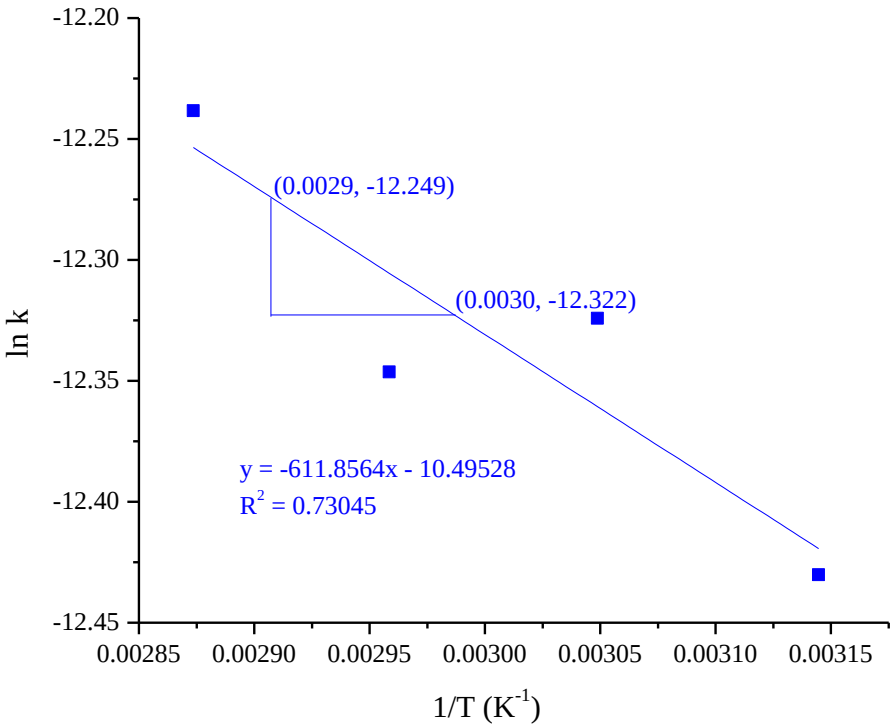

Fig. 4.14. Arrhenius plot (ln k versus 1/T) for first order reaction.

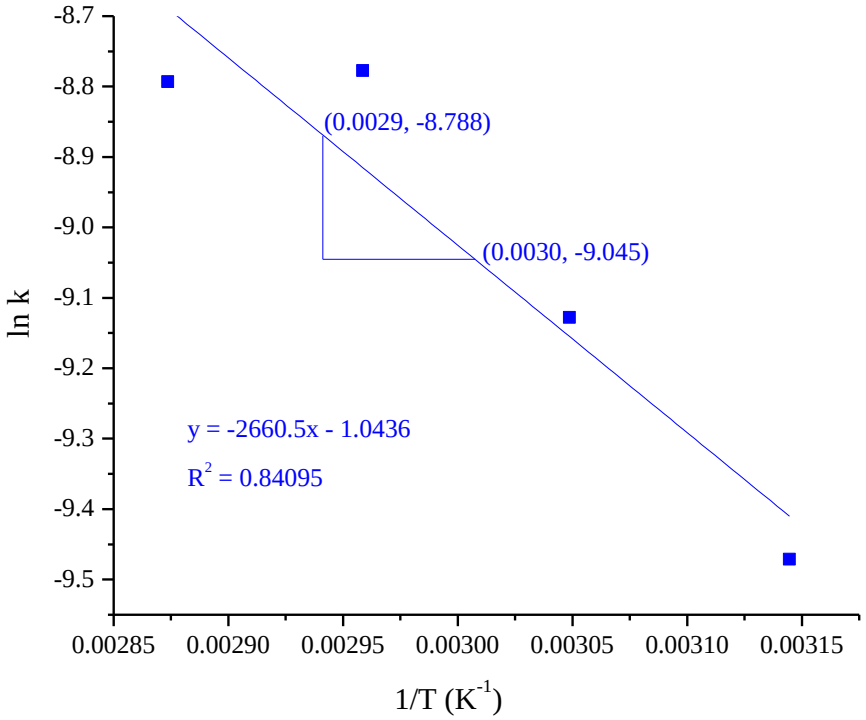

Fig. 4.15. Arrhenius plot (ln k versus 1/T) for pseudo-first order reaction.

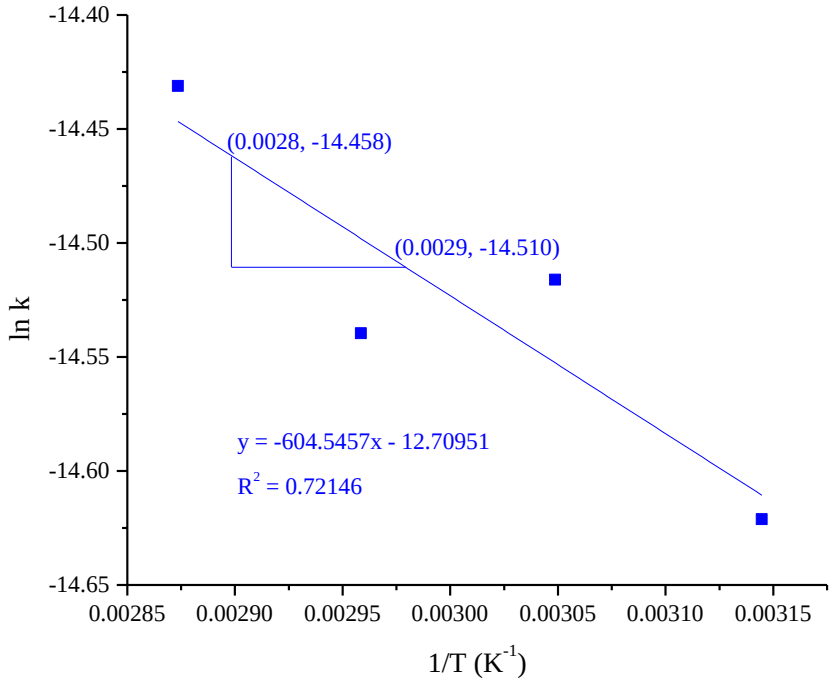

Fig. 4.16. Arrhenius plot (ln k versus 1/T) for second order reaction.

4.3.4 Thermodynamic study of the reaction

Based on Eyring-Polanyi equation (**4.9**) (Roy et al., 2020b; Banerjee et al., 2019), the values of thermodynamic parameters such as enthalpy change (ΔH^o) and entropy change (ΔS^o) were calculated from the slope (= $-\Delta H^o/T$) and intercept (= $\ln (k_b/h) + \Delta S^o/R$) of the Eyring-Polanyi graph of ln k/T versus 1/T (**Fig. 4.17**). The value of change in Gibb's free energy (ΔG^o) was calculated from the equation (**4.10**).

$$\ln\left(\frac{k}{T}\right) = -\left(\frac{\Delta H^o}{RT}\right) + \left[\ln\left(\frac{k_b}{h}\right) + \frac{\Delta S^o}{R}\right] \qquad (\mathbf{4.9})$$

$$\Delta G^o = \Delta H^o - T\Delta S^o \qquad (\mathbf{4.10})$$

where 'h' is the Planck constant (6.626×10^{-34} J.s) and 'k_b'is the Boltzmann constant (1.38×10^{-23} J K^{-1}).

The calculated value of ΔH^o is 19.35 kJ mol^{-1} K^{-1} and that of ΔS^o is –1.143 kJ mol^{-1} K^{-1}. This result ΔH^o with the positive value indicated that the reaction proceeds through the endothermic pathway and external heat supply. Roy et al. (2020b), Banerjee et al. (2019) and Sarve et al. (2016) also reported a positive value of ΔH^o in their studies showing the endothermic nature of the reaction. Similarly, ΔS^o with a negative value is reflecting the utilization of input energy and representing an endothermic reaction. The ΔG^o values of the

transesterification processes were found to be 382.96, 394.39, 405.82 and 417.26 kJ mol^{-1} at 318, 328, 338 and 348 K, respectively (Table S2), and these positive values are representing the non-spontaneous and endergonic nature of the reaction (Yahya et al., 2018).

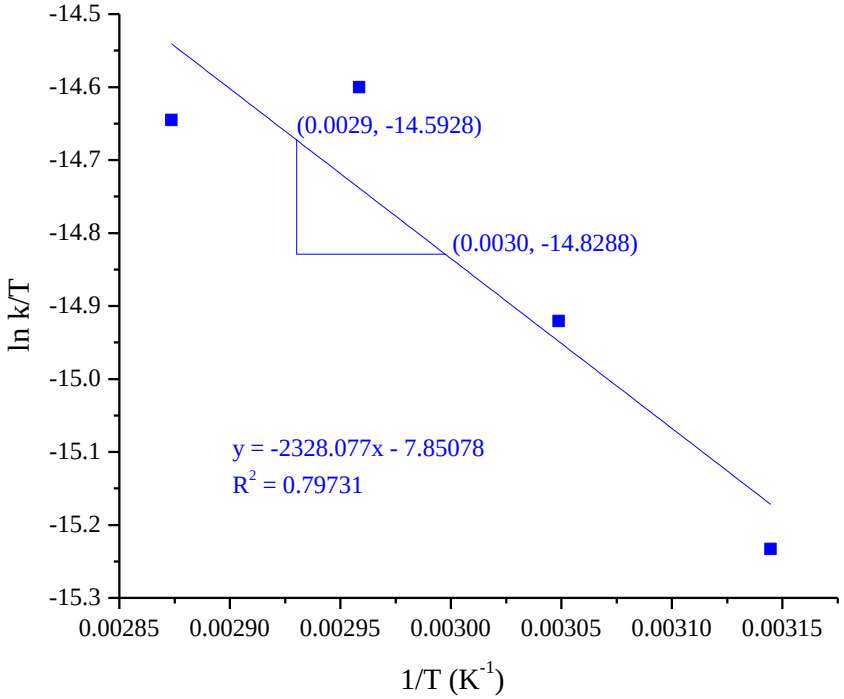

Fig. 4.17. Eyring-Polanyi plot (ln k/T versus 1/T).

Table 4.4: Thermodynamic parameters of the reaction

Thermodynamic parameters	**ΔH^o (kJ mol^{-1} K^{-1})**	**ΔS^o (kJ mol^{-1} K^{-1})**	**ΔG^o (kJ mol^{-1})**			
			318 K	**328 K**	**338 K**	**348 K**
Values	19.35	–1.143	382.96	394.39	405.82	417.26

4.3.5 Transesterification reaction mechanism

In this study, pH and basicity studies confirmed that the solid material derived from waste sugarcane bagasse is a base catalyst that contains a mixture of some inorganic bases like K_2CO_3, K_2O, CaO, and MgO along with other components. Hence, biodiesel production through transesterification using SBCC is a base-catalyzed reaction (**Scheme 4.1**). Roy et al. (2020a; 2020c) reported that transesterification reaction catalyzed by solid bases such as $BaSnO_3$ and K modified ceria oxide follows Eley-Rideal mechanism, and it was represented that the interaction of Ba–O or K–O bond with triglyceride molecule is more feasible where

the molecule is adsorbed rather than generating a nucleophile methoxide ion which is expected as a result of interaction between catalyst active species and methanol. Based on the Eley-Rideal mechanism, the plausible mechanism of biodiesel production via transesterification of the present investigation is illustrated in **Scheme 4.2**. At first, the active basic site M–O (K_2CO_3, K_2O, CaO, or MgO) present in the solid catalyst interacts with triglyceride, and adsorption takes place on the catalyst's surface. The formation of methyl esters takes place due to the surface interaction of methanol with adsorbed triglyceride. The third step involves the H–atom insertion to the adsorbed backbone of glycerol moiety leading to desorption of glycerol molecule. The catalyst's active site is restored and further interaction starts with the triglyceride molecule.

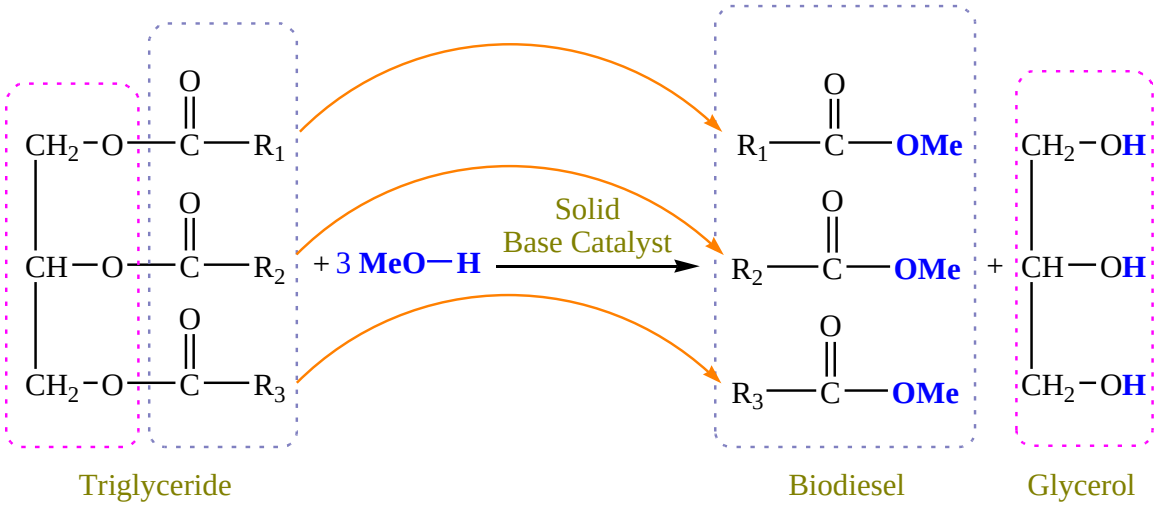

Scheme 4.1. Transesterification of triglyceride to biodiesel.

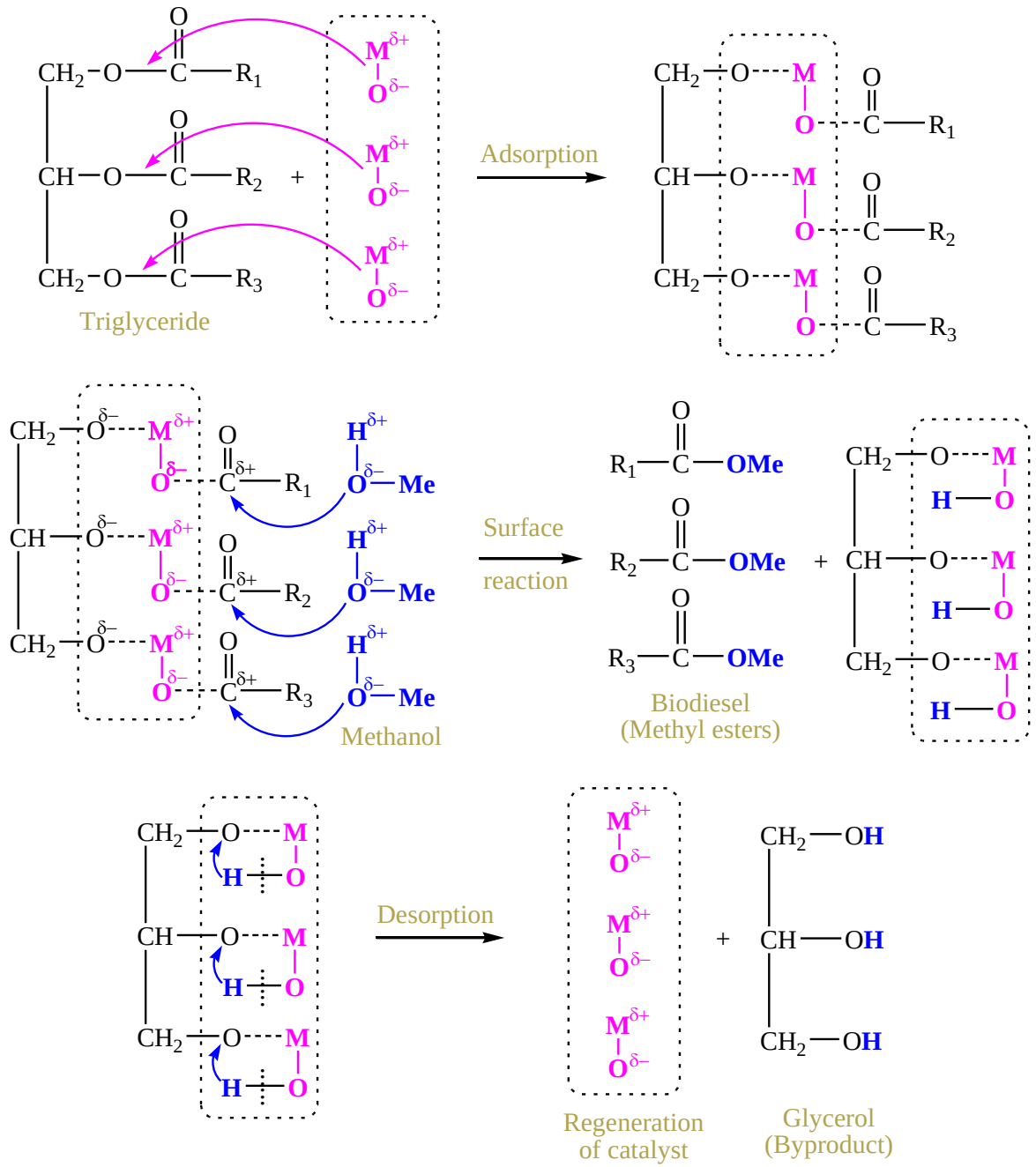

Scheme 4.2. Plausible transesterification mechanism for sugarcane bagasse derived solid base-catalyzed production of biodiesel.

4.3.6 Characterization of biodiesel

J. curcas oil and biodiesel were studied by ^{1}H NMR spectroscopy and the spectra are shown in **Fig. 4.18**. The chemical shift (δ) values of the ^{1}H NMR signals for different components of *J. curcas* oil and biodiesel are listed in **Table 4.5**. In ^{1}H NMR spectrum of oil (**Fig. 4.18** A), the signal at δ 5.267 ppm indicates the methine proton (-C***H***-CO_2R) at C2 of triglyceride, whereas there is no signal to signify the presence of methine proton in the ^{1}H NMR spectrum of biodiesel (**Fig. 4.18** B) indicating the conversion of oil to the product. Also, the methylene protons (-C***H***$_2$-CO_2R) at C1 and C3 of triglyceride are accredited by the signals at δ 4.120–4.318 ppm in ^{1}H NMR spectrum of oil (**Fig. 4.18** A) and these signals are disappearing in the spectrum of biodiesel (**Fig. 4.18** B) representing the transformation of oil to the product. The appearance of a new distinct signal at δ 3.650 ppm in the spectrum of biodiesel (**Fig. 4.18** B) is due to methoxy protons(-COOC***H***$_3$) of fatty acid methyl esters and is confirming the formation of biodiesel. The fatty acid composition of the synthesized biodiesel was characterized by the GC-MS technique. The chromatogram is shown in **Fig. 4.19** and the identified compositions are listed in **Table 4.6**. The fatty acid methyl esters detected were methyl oleate (79.58 %), methyl palmitate (16.26 %), methyl arachidate (1.51 %), methyl gondoate (0.76 %) and methyl palmitoleate (0.13 %).

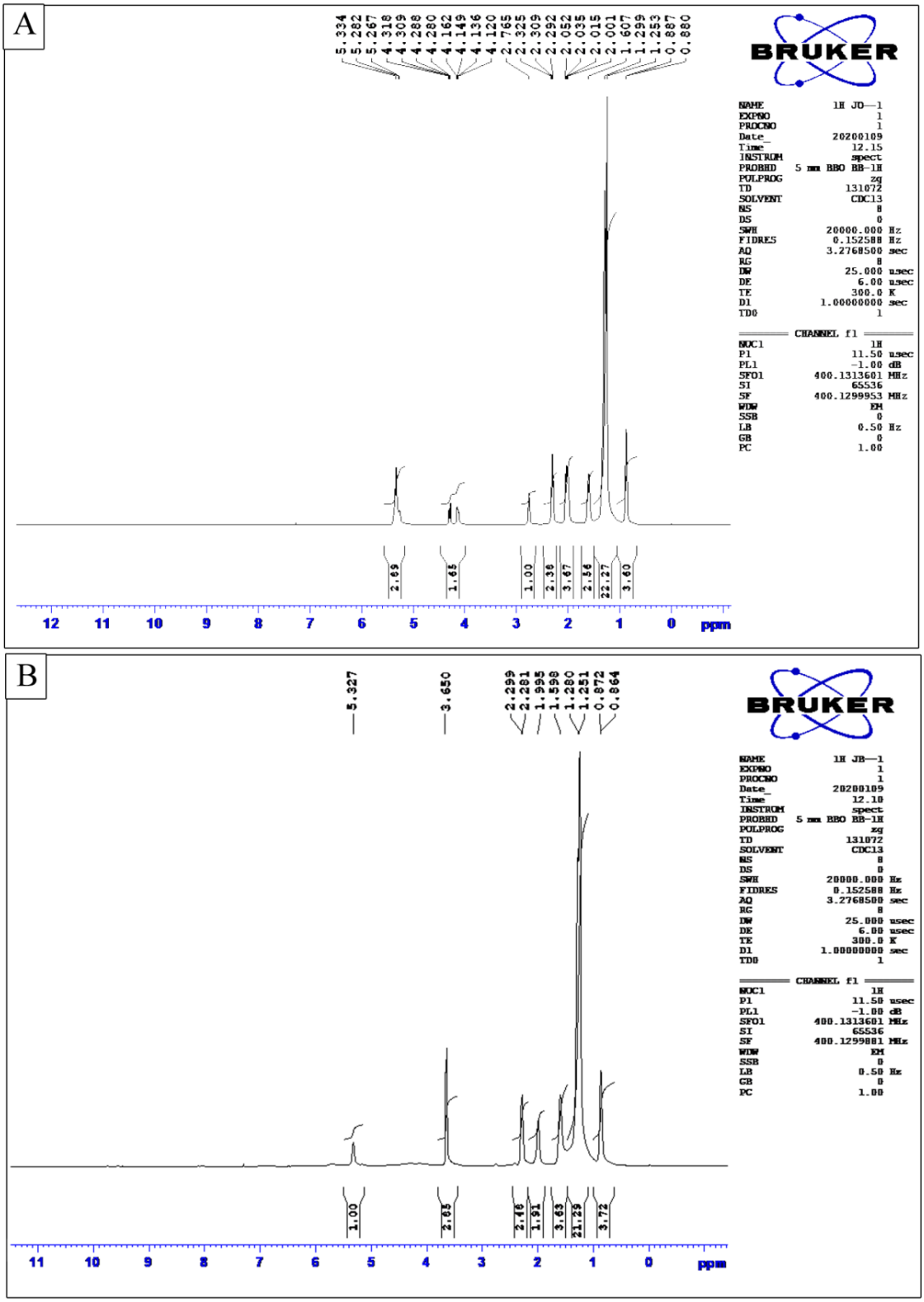

Fig. 4.18. ^{1}H NMR spectra of (A) jatropha seed oil and (B) biodiesel.

Table 4.5: NMR spectra analyses of *J. curcas* oil and biodiesel (Biodiesel).

Types of protons	***J. curcas* oil**	**Biodiesel**
	^{1}H NMR (δ, ppm)	**^{1}H NMR (δ, ppm)**
Olefinic protons (-C***H***=C***H***-)	5.282–5.334	5.327
Methine proton at C2 of glyceride (-C***H***-CO_2R)	5.267	–
Methylene protons at C1 and C3 of glycerides (-C***H***$_2$-CO_2R)	4.120–4.318	–
Methoxy protons (-COOC***H***$_3$) of esters	–	3.650
Bis-allylic protons (-C=C-C***H***$_2$-C=C-)	2.765	–
α-methylene to ester (-C***H***$_2$-CO_2R)	2.292–2.325	2.281–2.299
α-methylene to double bond (-C***H***$_2$-C=C-)	2.001–2.052	1.995
β-methylene to ester (C***H***$_2$-C-CO_2R)	1.607	1.598
Backbone methylenes -(C***H***$_2$)$_n$-	1.253–1.299	1.251–1.280
Terminal methyl protons (C-C***H***$_3$)	0.880–0.887	0.864–0.872

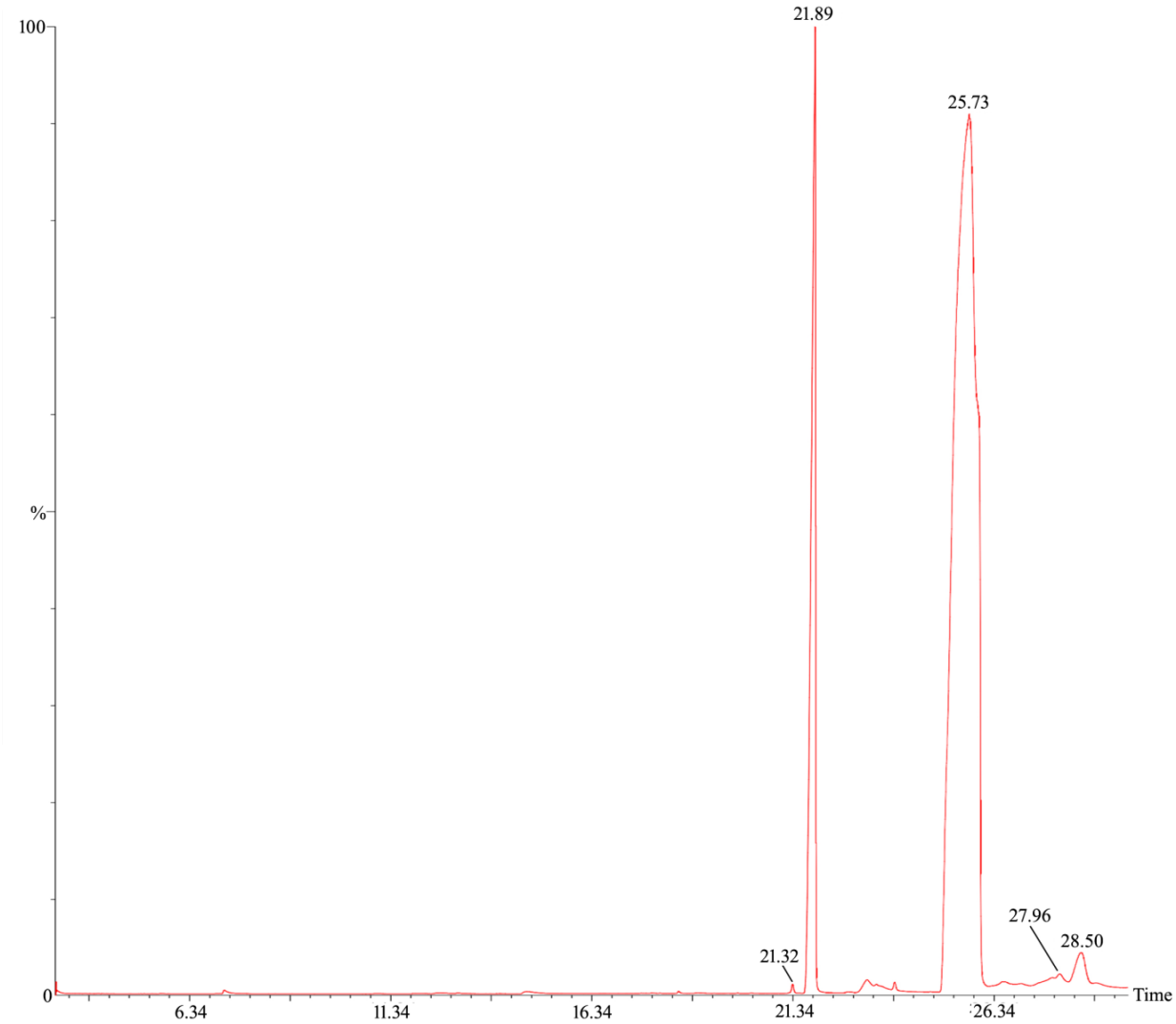

Fig. 4.19. Gas chromatogram of biodiesel.

Table 4.6: GC-MS analysis of biodiesel.

Retention time	Fatty acid methyl esters	Composition (%)
21.32	Methyl palmitoleate (C16:1)	0.13
21.89	Methyl palmitate (C16:0)	16.26
25.73	Methyl oleate (C18:1)	79.58
27.96	Methyl gondoate (C20:1)	0.76
28.50	Methyl arachidate (C20:0)	1.51

4.3.7 Fuel properties of biodiesel

The properties of biodiesel and reported biodiesel are presented in **Table 4.7**. The density of biodiesel at 29 ^{o}C is found to be 0.874 g cm^{-3} and comparable with the values reported by Pathak et al. (2018) and Nath et al. (2020) for soybean biodiesel and sunflower biodiesel, respectively. However, a slightly higher density of 0.9 g cm^{-3} was reported by Yahya et al. (2018) for waste cooking oil biodiesel. The kinematic viscosity of fuel which is responsible for the smooth flow of the biodiesel in the engine was determined and found to be 5.659 mm^2 s^{-1}, and is within the specified range of ASTM D6751. Kinematic viscosities of 5.98 mm^2 s^{-1} (soybean biodiesel), 5.0 mm^2 s^{-1} (*Azadirachta indica*) and 5.2 mm^2 s^{-1} (used cooking oil biodiesel) were reported by Pathak et al. (2018), Etim et al. (2018) and Yahya et al. (2018), respectively. The specific gravity of biodiesel was found to be 0.854, and is comparable to the reported values of biodiesel from *Azadirachta indica* (Etim et al., 2018), *Bauhinia monandra* (Betiku et al., 2016) and palm oil (Odude et al., 2019). The SN and iodine value were found to be 191.84 mg KOH/g and 70.24 g I_2/100 g, respectively. Low saponification value indicates a lower proportion of fatty acids with low molecular weight in the oil or biodiesel (Diwakar et al., 2010; Ismail and Ali, 2015). Iodine value is an essential specification of biodiesel that expresses unsaturation in the oils or fats, and the fuel with a low amount of iodine value is considerably preferred (Diwakar et al., 2010). The quality of biodiesel is said to be excellent when it has a high cetane index because the biodiesel with a higher cetane index displays better ignition quality and emits less harmful gases (Perea et al., 2016). In this study, the cetane index was calculated and found to be 58.95 for biodiesel. A high cetane index of 59.23 with a high cetane number of 55.5 was reported for jatropha biodiesel (Basumatary et al., 2021c). This indicates that the cetane index which is calculated from the fatty acid composition can predict the cetane number of biodiesel, and comparable data is achievable. In this study, the HHV of biodiesel is determined and found to be 40.51 MJ/kg indicating good fuel as it possibly can produce a high amount of heat compared to petrodiesel (Deka and Basumatary, 2011). Biodiesels produced from sunflower oil (Nath et al., 2020), used cooking oil (Yahya et al., 2018), *Bauhinia monandra* oil (Betiku et al., 2016) and *J. curcas* oil (Basumatary et al., 2021c) have been reported with comparable HHV. The calculated API, diesel index and aniline point (^{o}F) were 34.28, 67.98 and 198.33, respectively.

Table 4.7: Properties of biodiesel.

Parameter	**Biodiesel (This study)**	**ASTM D6751**	**Reported biodiesel**						
			Soybean (Pathak et al., 2018)	***Azadirachta indica*** (Etim et al., 2018)	***Bauhinia monandra*** (Betiku et al., 2016)	**Sunflower** (Nath et al., 2020)	**Palm** (Odude et al., 2019)	**Used cooking oil** (Yahya et al., 2018)	**Jatropha** (Basumatary et al., 2021c)
Density (g/cm^3)	0.874	0.86–0.90	0.857	-	-	0.859	-	0.90	0.878
Kinematic viscosity (mm^2/s)	5.659	1.9–6.0	5.98	5.0	4.90	3.11	4.3	5.2	3.624
Specific gravity	0.854	0.86–0.90	-	0.88	0.876	-	0.86	-	-
SN (mg KOH/g)	191.84	-	-	-	-	188.57	-	188.2	191.64
Iodine value (g I_2/100 g)	70.24	NS	-	58.6	52.22	-	40.90	-	69.11
Cetane index	58.95	-	-	-	-	-	-	-	59.23
HHV (MJ/kg)	40.51	NS	-	48.7	43.19	39.79	-	39.04	40.53
API	34.28	36.95	-	-	30.03	34.277	32.42	-	34.28
Diesel index	67.98	50.4	-	-	69.21	50.82	92.95	-	68.37
Aniline point (^{o}F)	198.33	331	-	-	-	148.27	-	-	199.47

NS–Not specified; SN–Saponification number; API–American petroleum index; HHV–Higher heating value.

4.4 Conclusion

A renewable low-cost solid catalyst was prepared from waste sugarcane bagasse and applied for the synthesis of biodiesel. The analysis revealed that the catalyst is composed of various metal oxides and carbonates. The micro-mesoporous and polycrystalline nature of this catalyst contained a low surface area of 7.66 m^2 g^{-1}. The catalyst produced 92.84 wt. % of biodiesel at 9:1 MTOMR, 10 wt. % catalyst and 65 ^oC in 285 min. The catalyst is basic in nature with basic strength of 10.1 < H_ < 18.4, and possesses good efficacy for the reaction with TOF of 6.59 h^{-1} and E_a value of 22.12 kJ mol^{-1}. The thermodynamic study indicated the non-spontaneous and endothermic nature of the reaction. Due to abundant availability, renewability and high economic viability, waste sugarcane bagasse has the potential to be developed as a cheap base catalyst for biodiesel production at a large-scale along with the development of other materials for sustainable applications."